Drawn-polymer recuperative heat exchangers for use in cryocoolers

Drawn-polymer recuperative heat exchangers for use in cryocoolers

Drawn-polymer recuperative heat exchangers for use in cryocoolers

J L Adams[1], K J Thompson[2], J Cummings[2], L Cantley[2], and J G Brisson[1]

[1]Massachusetts Institute of Technology, Cambridge MA
[2]MIT Lincoln Laboratory, Lexington MA

Email: jacoba@mit.edu

Abstract. Polymer microchannel heat exchangers for use in cryocooler applications have been developed. These heat exchangers are manufactured using a thermal drawing process where a bulk polymer preform is heated and stretched. The process results in channels with a characteristic dimension of 50-100 µm and with an overall length of many meters. The drawn heat exchangers are lightweight, flexible, and have a large surface-area-to-volume ratio. Initial tests on a Joule-Thomson cryocooler with a heat exchanger of overall dimension of 2.5mm x 2.5mm x 420mm with nitrogen as a working fluid were performed. Nitrogen was successfully liquified with a mass flow rate of 34 mg/s and cooling power of 200 mW at 80 K.

1. Introduction

Cryocoolers rely on high performance heat exchangers, which in most cases are constructed with flow passages on the order of 1-10 mm. Some applications benefit from even smaller flow passages, micro-channels, on the order of 10-100 µm. The decrease in channel size allows for an increase in the heat transfer area per unit volume resulting in a more compact heat exchanger [1]. A common method of producing micro-channeled heat exchangers for cryogenic applications is through photo-chemically etching on glass, silicon, or metals [2]. There are drawbacks to the photo-chemical manufacturing method including expensive dies, rigid or brittle heat exchangers (in the case of glass or silicon), and short overall channel lengths (1-10 cm length).

Micro-channels can also be created using a drawing process. Recently, advanced thermally drawn polymer fibers with complex micro-structures have been developed for use in a variety of applications ranging from wearable electronics to microfluidic high-throughput cell separation [3]. This work uses a drawn polymer as a new type of counterflow heat exchanger.

The drawn polymer manufacturing method allows for a macro-scale preform to be machined using conventional techniques at the millimeter scale, and then reduced to the micrometer scale through a drawing process. Geometrical features as small as 10 µm can be achieved. The drawn polymer manufacturing technique has many advantages including: 10’s to 100's of meter of channel length, low material cost, thin walls, fine micro-structure, and low axial heat conduction. Despite their low thermal conductivity, polymers are well suited to micro-channeled applications since thin walls allow for an overall thermal conductance comparable to the conductance of laminar-flowing fluid in a micro-channel (see section 3.2). This work applies these manufacturing and material advantages to heat exchangers.

A proof of concept drawn polymer heat exchanger was designed, manufactured, and tested in a Joule-Thomson (JT) cryocooler. The heat exchanger is constructed with polyetherimide (PEI) and demonstrates leak-free operation with high-pressure nitrogen gas (up to 15 MPa). The drawn polymer JT cryocooler was successful in liquefying nitrogen. A cooling power of 200 mW was measured at a temperature of 80 K with a mass flow rate of 34 mg/s.

Future drawn polymer heat exchangers may employ cross-flow structures or configure many drawn polymers in parallel for increased flow rates. Alternatively, this work may inspire the use of drawn polymers to adjacent thermal applications such as regenerative heat exchangers, or heat pipes.

2. Fabrication of Drawn Polymer Heat Exchanger

The typical manufacturing process for a drawn polymer is graphically shown in figure 1 and described in short here:

1. Machine layers: Polymer sheets are machined with channels on the millimeter scale. Teflon spacers are laser cut to fit within the machined channels.
2. Thermally consolidate preform: The polymer layers and corresponding Teflon spacers are stacked appropriately to create the un-bonded preform. The preform is consolidated in a hot press. The Teflon spacers do not bond to the polymer and are removed afterwards.
3. Draw preform: The consolidated preform is mounted in the draw tower. The draw tower is comprised of an open-ended oven that heats the preform. The preform softens/flows and the fiber is collected at the end by a spool.
4. Header the drawn polymer: The drawn polymer is machined and headered with collars, so that working fluid can be directed into and out of the micro-channels.

Alternative manufacturing techniques or steps are discussed by Reference [3].

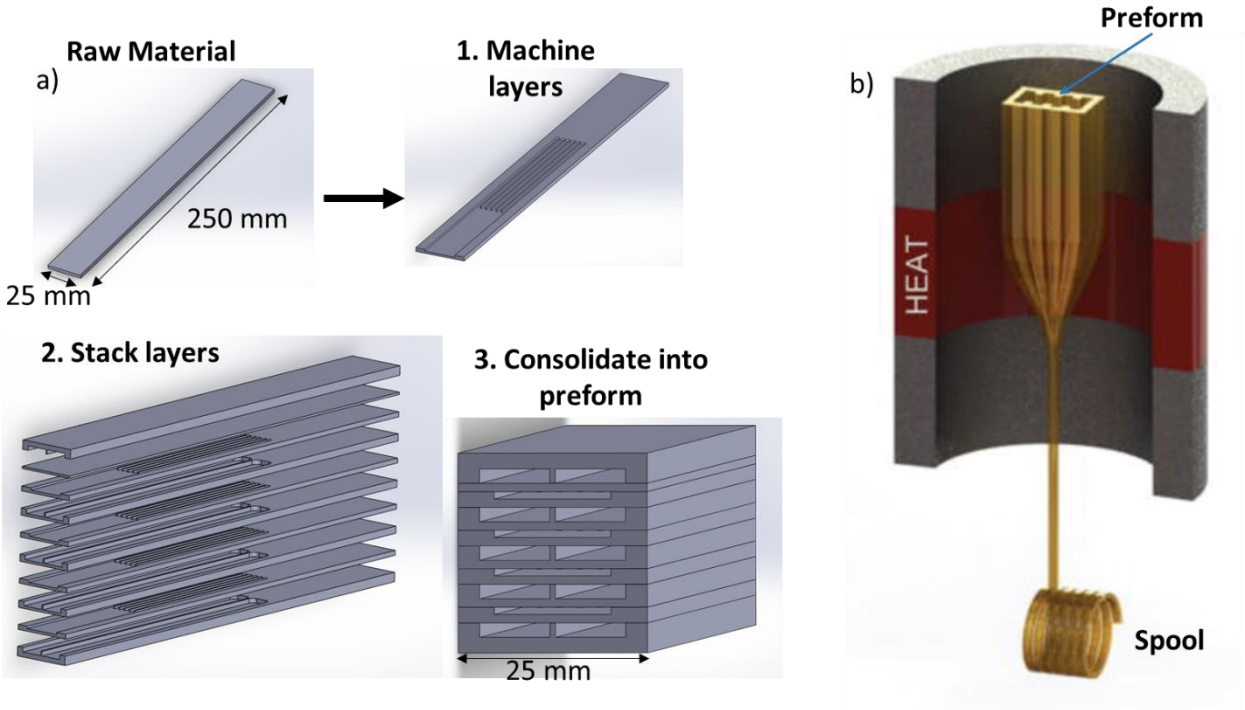

Figure 1: Manufacturing process for a thermally drawn polymer. Preform steps 1-3 labelled: Step 1. Machine layers, Step 2. Stack layers, Step 3. Consolidate into preform. Teflon spacers omitted. b) Conceptual layout of draw tower with heated oven that draws the preform [4].

2.1. Drawn Polymer Headering

The low-pressure and high-pressure micro-channels inside the drawn polymer need to be accessed separately. To do this, the larger low-pressure channels are accessed from the sides of the drawn polymer, while the smaller high-pressure channels are accessed from the ends. In our process, the low-pressure channels extend 125 μm beyond the high-pressure channels allowing for preferential access from the sides by machining off ~200 μm using an end mill on a high speed Dremel tool (see Figure

2a). To access only the high-pressure channels from the ends, the low-pressure channels are internally plugged with epoxy for a ~1cm length so that only the high-pressure channels are open to the ends.

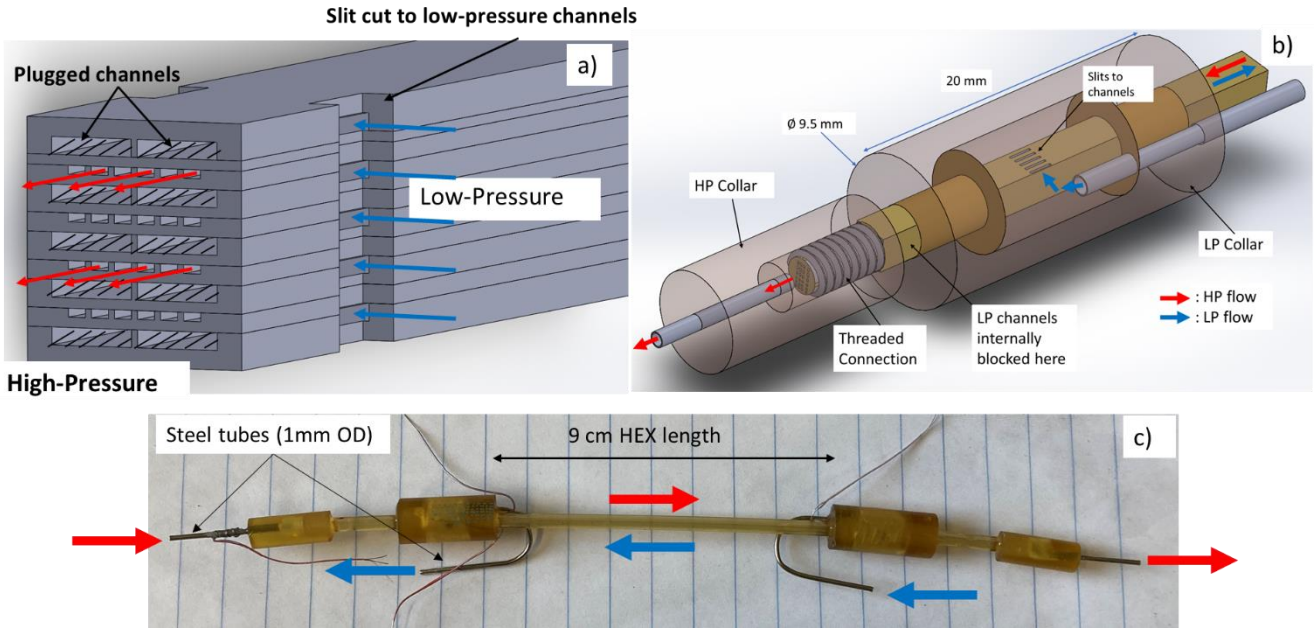

Figure 2: a) Diagram detailing low-pressure (LP) fluid entering drawn polymer from the side, while the high-pressure (HP) fluid is exiting from ends. b) 3d model depicting collar design with flow paths labeled. c) Image of completed drawn heat exchanger with 9 cm long heat exchange portion.

After the drawn polymer has been selectively machined and internally plugged in the correct locations, PEI collars are slid over the drawn polymer. The collars are sealed around the drawn polymer with epoxy (Stycast 1266), and direct gas flow into the micro-channels. Thin walled stainless-steel capillary tubes (1mm OD) are inserted into the collars and sealed with epoxy. External connections are made to the steel tubes.

3. Joule-Thomson Cycle and Heat Exchanger Thermal-Hydraulic Performance

As a test of concept, a drawn heat exchanger was designed for use in a Joule-Thomson (JT) cryocooler with high-pressure (11 MPa) nitrogen working fluid. Nitrogen was chosen as the working fluid since it can cool from room temperature (300 K) all the way to cryogenic temperatures (77 K) in a single stage. The target cooling power was 500 mW to overcome parasitic heat loads.

3.1. Joule-Thomson Cycle

The Joule-Thomson (JT) cryocooler (diagrammed schematically in figure 3) reaches cryogenic temperatures with the help of a recuperative heat exchanger which pre-cools the incoming warm, high-pressure fluid (1→2) with the outgoing cold, low-pressure fluid (4→5). After the high-pressure gas exits the heat exchanger at state 2, it expands through an isenthalpic (constant enthalpy) throttle (i.e. $h_2 = h_3$). This expansion process provides the elementary cooling effect which drives the JT cycle. Finally, the working fluid absorbs the cooling load, $\dot{Q}_{cooling}$, from state 3→4 before returning to the heat exchanger.

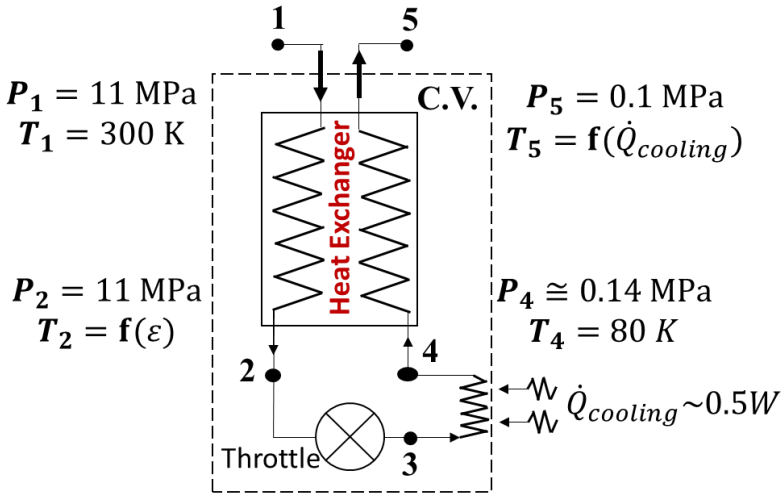

Figure 3: Diagram of JT cryocooler with statepoints labelled. Nominal operating conditions used in experimental Section 4 are labelled. Control volume (C.V.) marked with dotted line.

Applying the conservation of energy to the control volume (C.V.) in Figure 3

$$\dot{Q}_{cooling} = \dot{m}(h_5 - h_1) \tag{1}$$

where $\dot{m}$ is the mass flow rate, h_1 and h_5 are the enthalpies at states 1 and 5 respectively. The maximum cooling power of this JT cryocooler occurs when the temperature at state 5 equals the temperature at state 1 (i.e. $T_1 = T_5$). The maximum cooling power for a nitrogen JT cryocooler with the given inlet and outlet conditions shown in figure 3 with a mass flow rate of 34 mg/s is 700mW, close to the desired cooling power of 500 mW (the enthalpies are evaluated using Refprop).

3.2. $\varepsilon - NTU$ Method

The heat exchanger thermal performance is predicted using the $\varepsilon - NTU$ method assuming average fluid properties over the temperature range. For a counterflow heat exchanger, the effectiveness (ε) is a function of the Number of Transfer Units (NTU) and the flow capacity ratio (C_r) [5].

$$NTU = \frac{UA}{C_{min}} \tag{2}$$

$$\varepsilon = \frac{\dot{Q}_{actual}}{\dot{Q}_{max}} = \frac{1-e^{-NTU(1-C_r)}}{1-C_r e^{-NTU(1-C_r)}} \tag{3}$$

Where C_r is the ratio between the minimum flow capacity rate over the maximum flow capacity rate ($C_r = \frac{C_{min}}{C_{max}}$). U is the overall heat transfer coefficient, and A is the surface area for heat transfer.

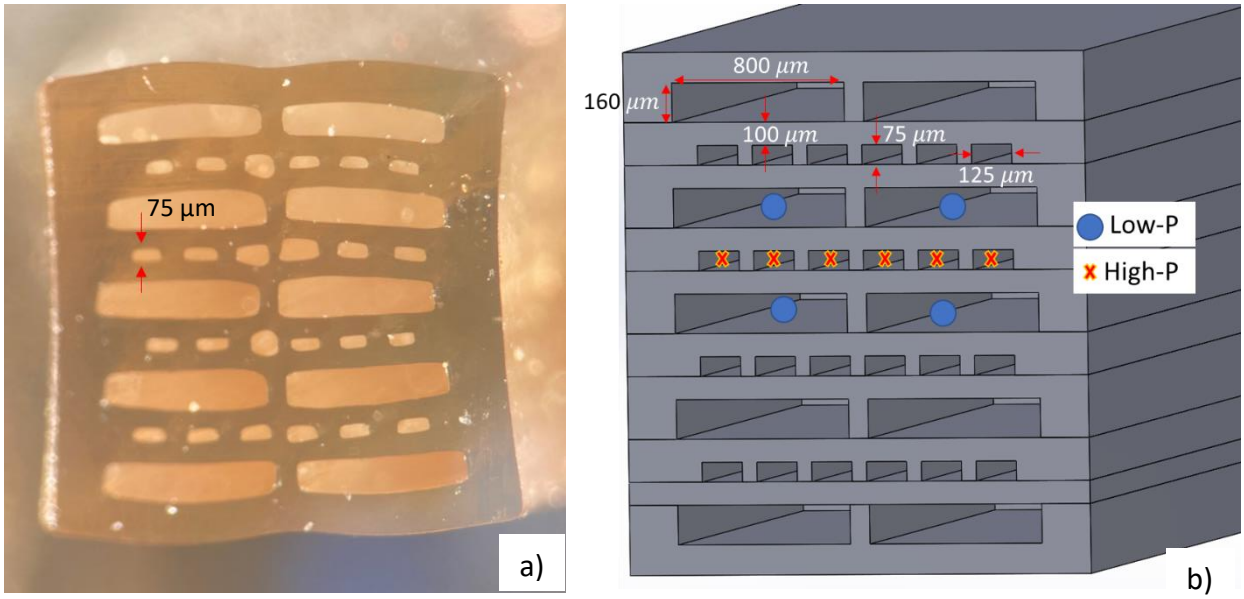

Figure 4: a) Cross-sectional image of drawn polymer. b) Cross-sectional drawing with dimensions used in modeling. Labelled dimensions are measured on the actual drawn polymer shown in a).

The overall heat transfer coefficient is determined by modeling the two fluid flows separated by a solid wall. In this case, the heat transfer is through three thermal resistances in series. There is the resistance of convection for both the low-pressure ($R_{LP} = \frac{1}{\hbar_{LP}}$) and high-pressure fluids ($R_{HP} = \frac{1}{\hbar_{HP}}$), in series with the resistance of conduction across the separating polymer wall ($R_{wall} = \frac{t_{wall}}{k_{wall}}$). Where $\hbar$ is the heat transfer coefficient, t_{wall} is the wall thickness, and k_{wall} is the thermal conductivity of the wall. For these three thermal resistances in series, U is given by

$$U = \left(\frac{1}{\hbar_{HP}} + \frac{t_{wall}}{k_{wall}} + \frac{1}{\hbar_{LP}}\right)^{-1} \tag{4}$$

Drawn heat exchangers generally have small hydraulic diameter, D_h, channels and the fluid flow in these channels is usually laminar. The Nusselt number, Nu, relation is used to find the heat transfer coefficient, $\hbar$. For laminar flow, the Nusselt number will have a characteristic value of 4 (depending on geometry and boundary conditions, the Nu will range between values between 2 and 8) [5].

For a channel under laminar flow conditions, the pressure drop, ΔP, is given by

$$\Delta P = \frac{C_1 \mu}{2\rho} \frac{L}{D_h^2 A_c} \dot{m} \tag{5}$$

where A_c is the cross-sectional area of the channel, μ is the fluid viscosity, and C_1 is a constant that depends on the shape of the channel (for example $C_1 = 64$ for a circular channel).

Table 1. Thermal-hydraulic performance of modelled heat exchanger.

	Low-pressure (0.1 MPa)	High-pressure (10 MPa)	Wall (100 µm)
Nusselt number	5.7	3.9	N/A
$R_{Thermal}$ ($\frac{m^2-K}{W}$)	2.7x10^{-3}	0.7x10^{-3}	0.5x10^{-3}
ΔP (kPa)	42	27	N/A

Length	42 cm
$\dot{m}$	34 mg/s
C_r	0.72
UA	0.62 W/K
NTU	18
Effectiveness (ε)	0.998

Table 1 shows the thermal-hydraulic performance of the drawn polymer heat exchanger for the defined geometry in figure 4. For an appropriate heat exchanger design, the thermal resistance of the wall, should be the same or less than the thermal resistance of the fluid flows. Table 1 indicates that the thermal resistances of the wall is on par with the fluids. Therefore, the low thermal conductivity of the polymer does not substantially inhibit heat transfer because the wall thermal resistance is comparable to that of the laminar-flow fluids (in part due to the thin, 100 µm walls).

For the capacity ratio, $C_r = 0.72$, and number of transfer units, $NTU = 18$, equation 3 gives an effectiveness of $\varepsilon = 0.998$. This is an optimistic calculated effectiveness (model does not consider non-ideal effects such as flow maldistribution), yet it indicates that there is adequate thermal conductance for high performance.

4. Experimental Performance of Drawn Polymer Heat Exchanger

The experimental goal is to demonstrate the function of the drawn polymer heat exchanger in a Joule-Thomson (JT) cryocooler.

4.1. Experimental Setup

The drawn heat exchanger is headered as described in section 2.1. The cryocooler is suspended in vacuum to reduce parasitic heat loads as shown below in figure 5. The cryocooler is supplied with 300 K high-pressure, high-purity (99.99%) nitrogen gas from a cylinder. A mass flow meter calibrated for nitrogen (Omega FMA1700A) measures the flow rate at the outlet. The nitrogen gas is vented to atmosphere.

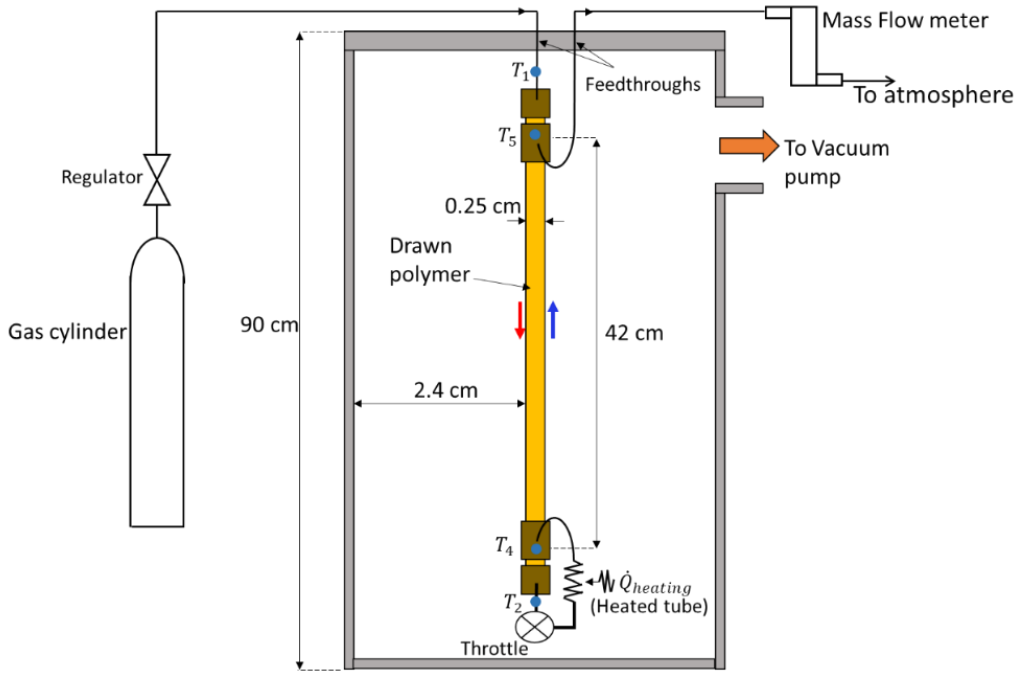

Figure 5: Schematic of drawn heat exchanger suspended in vacuum chamber with relevant dimensions labelled. Location of thermocouples indicated.

The cryocooler is instrumented with 34-gauge special limits of error ($\pm$1 K) E-type thermocouples at statepoints 1, 2, 4, and 5 (locations shown in figure 5). E-type thermocouples are sensitive down to 40 K. To confirm that the thermocouples read accurately in the temperature range of interest, the cryocooler was submerged in atmospheric liquid nitrogen where all thermocouples read ~77.3 K (within ~0.2 K of each other).

A wound 0.4 m long, 125 µm ID copper-nickel capillary serves as the throttle. A large diameter throttle was chosen to reduce the likelihood of impurity clogging. A segment of heated tube applies the heating power ($\dot{Q}_{heating}$) to the working fluid. This heated tube consists of a twisted pair of 36-gauge maganin wire wrapped around a 2-inch long, 800 µm OD (500 µm ID) stainless-steel tube. The maganin wire serves as a resistance element (100 Ω) that equally distributes heat along the entire tube length. The temperature on the outside of the heated tube was monitored with an E-type thermocouple.

4.2. Results

Figure 6 shows a cooldown curve (plot of temperature versus time) and the temperature response of statepoints 2, 4, and the heater temperature under various heating powers. Figure 6 shows the temperature at state 2 falling from 150 K to 83 K over a 60-minute period. The temperature measurements give insight into the flow conditions. The first observation is that when heat is applied at both 100 mW and 200 mW, the temperature at state 4 remains constant. This indicates a two-phase mixture at constant pressure, with both liquid and gaseous nitrogen returning to the recuperator at state 4.

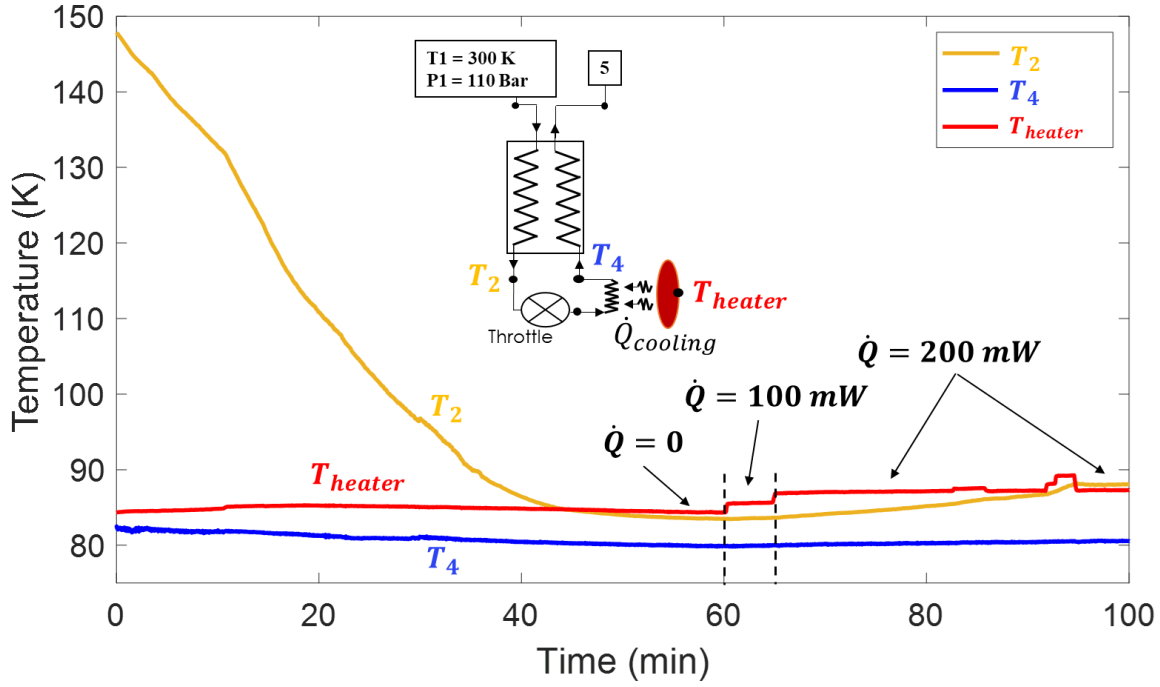

Figure 6: Temperature versus time cooldown curve for JT cryocooler experiment. Various applied heater powers are labeled. Notice that the heater temperature (red line) increases as more heat is applied, while the temperature of state 4 (blue line) stays constant. The measured mass flow rate is 34 mg/s.

In addition to the cooldown curve shown in figure 6, this cryocooler was also able to maintain $T_4 = 80\ K$ at a reduced inlet pressure of 8 MPA (flow rate of 28 mg/s) with zero heater power.

The effectiveness of the drawn polymer heat exchanger is estimated using the measured statepoint temperatures in figure 6 (at a heating power of 200 mW) and the definition of effectiveness (equation 3). The effectiveness is estimated to be 0.96 ± 0.015. The error is determined from a 1 K uncertainty in temperature measurements.

The measured effectiveness, 0.96 ± 0.015, does not match the predicted effectiveness of 0.998 (table 1). The discrepancy between measured and predicted effectiveness is, in part, due to radiative losses along the heat exchanger which are estimated to be ~500 mW out of the total 13 W transferred (4%). Additionally, thermal performance detriment from flow maldistribution amongst the micro-channels was not considered in the $\varepsilon - NTU$ modeling of section 3.2. It is well known that flow

maldistribution in real heat exchangers reduces thermal effectiveness, especially in the case of high NTU heat exchangers with many parallel flow passages [6].

The measured saturation temperature at state 4 is 80 K, corresponding to a saturation pressure of 150 kPa. Since the outlet pressure at state 5 is atmospheric (101 kPa), the pressure drop between state 4 and 5 is 49 kPa. The predicted pressure drop for this flow rate (34 mg/s) and operating condition is 42 kPa (Table 1), giving good agreement between the two values.

5. Conclusions

A novel micro-channeled recuperative heat exchanger was manufactured from a drawn polymer for application to Joule-Thomson cryocoolers. The drawn polymer has adequate dimensional stability to be used as an effective heat exchanger. A headering scheme was developed that allowed for fluids to be directed into and out of the drawn polymer. The headering scheme and drawn polymer was leak tight to nitrogen at high pressures (up to 15 MPa) over many temperature cycles spanning 300 K to 80 K.

The drawn heat exchanger was experimentally validated by successfully liquefying nitrogen in a Joule-Thomson cryocooler. The cryocooler was capable of 200 mW of cooling power at 80 K with a mass flow rate of 34 mg/s.

Drawn polymers can be used as recuperative heat exchangers in cryocooler applications. Future developments may build upon this work to integrate the drawn polymer heat exchanger into applications that can benefit from lightweight, low-cost, and flexible heat exchangers. Additionally, drawn polymers can be designed for use in adjacent thermal applications including regenerators or heat pipes.

6. References

[1] Y. Fan and L. Luo, and G. Flamant (2013), “Design of Compact Heat Exchangers for Transfer Intensification.” *Springer London*
[2] W. A. Little (1982), “Microminiature refrigeration - small is better.” *Physica B+C*
[3] W. Yan et al. (2020), “Thermally drawn advanced functional fibers: New frontier of flexible electronics.” *Materials Today*
[4] R. A. Koppes et al. (2016), “Thermally drawn fibers as nerve guidance scaffolds.” *Biomaterials*
[5] W. M. Kays and A. L. London. (1958), “Compact Heat Exchangers.” *McGraw-Hill*
[6] R. B. Fleming (1967), “The effect of flow distribution in parallel channels of counterflow heat exchangers.” *Advances in Cryogenic Engineering*

Acknowledgments

This material is based upon work supported by the Under Secretary of Defense for Research and Engineering under Air Force Contract No. FA8702-15-D-0001. Any opinions, findings, conclusions or recommendations expressed in this material are those of the author(s) and do not necessarily reflect the views of the Under Secretary of Defense for Research and Engineering. Delivered to the U.S. Government with Unlimited Rights, as defined in DFARS Part 252.227-7013 or 7014 (Feb 2014). Notwithstanding any copyright notice, U.S. Government rights in this work are defined by DFARS 252.227-7013 or DFARS 252.227-7014 as detailed above. Use of this work other than as specifically authorized by the U.S. Government may violate any copyrights that exist in this work.